nature structural & molecular biology

Structure of Nipah virus unassembled nucleoprotein in complex with its viral chaperone

Filip Yabukarski[1,2], Philip Lawrence[3], Nicolas Tarbouriech[1,2], Jean-Marie Bourhis[1,2], Elise Delaforge[4–6], Malene Ringkjøbing Jensen[4–6], Rob W H Ruigrok[1,2], Martin Blackledge[4–6], Viktor Volchkov[3] & Marc Jamin[1,2]

Nipah virus (NiV) is a highly pathogenic emergent paramyxovirus causing deadly encephalitis in humans. Its replication requires a constant supply of unassembled nucleoprotein (N^0) in complex with its viral chaperone, the phosphoprotein (P). To elucidate the chaperone function of P, we reconstituted NiV the N^0–P core complex and determined its crystal structure. The binding of the N-terminal region of P blocks the polymerization of N by interfering with subdomain exchange between N protomers and keeps N^0 in an open conformation, ready to grasp an RNA molecule. We found that a peptide derived from the N-binding region of P protects cells against viral infection and demonstrated by structure-based mutagenesis that this peptide acts by inhibiting N^0–P formation. These results provide new insights about the assembly of N along genomic RNA and validate the N^0–P complex as a target for drug development.

© 2014 Nature America, Inc. All rights reserved.

The Paramyxoviridae are a large family of nonsegmented negative-strand RNA viruses (NNVs) associated with human respiratory illnesses (for example, respiratory syncytial virus (RSV) and human parainfluenza viruses) and with common childhood diseases such as measles and mumps. Owing to phylogenetic relationships, Paramyxoviridae are divided in two subfamilies, the Paramyxovirinae and the Pneumovirinae, and are classified in the order Mononegavirales with the families Rhabdoviridae, Bornaviridae and Filoviridae[1]. NiV is emblematic of emerging viruses; spilling over from its natural bat hosts in South East Asia, this virus causes outbreaks of respiratory and encephalic diseases in various mammals including humans[2]. Because of its mortality rate that can exceed 70% in humans, its potential for human-to-human transmission and the absence of vaccine or specific antiviral treatment, NiV is classified among biosafety level 4 (BSL-4) pathogens.

The genomic RNA of NiV, like that of all NNVs, is condensed by a homopolymer of nucleoprotein (N), forming long helical nucleocapsids (NCs). These ribonucleoprotein complexes are the biologically active templates used for RNA synthesis by the viral RNA-dependent RNA polymerase[3,4]. Consistently with the ability of the NNV NCs to protect genomic RNA against nucleases, the N proteins comprise two globular domains, the N-terminal (N_{NTD}) and C-terminal (N_{CTD}) domains, that completely enwrap the RNA molecule[5–8] (**Fig. 1a**). The N homopolymer is stabilized by lateral contacts and the exchange of N-terminal (NT_{ARM}) and C-terminal subdomains (CT_{ARM}) between adjacent protomers[5–8]. In the Paramyxovirinae subfamily, N has an additional long disordered C-terminal tail (N_{TAIL}) that extends outside the NC and binds to the P C-terminal domain (P_{XD})[9–11]. The tight packaging of the RNA has prompted the hypothesis that N must open and close to accommodate RNA inside the binding groove during NC assembly and to transiently release the RNA template upon passage of the RNA polymerase, but until now there has been no evidence of a conversion between open and closed N forms.

In the absence of other viral proteins, N has a strong tendency to polymerize and to assemble on cellular RNAs. In Paramyxoviridae, but also in Rhabdoviridae and perhaps in all NNVs, viral protein P acts as a specific chaperone of nascent N and keeps it in an assembly-competent form (N^0) by preventing both N polymerization and its interaction with cellular RNAs[12,13]. Paramyxoviridae and Rhabdoviridae P proteins are modular multifunctional proteins, which comprise a long intrinsically disordered N-terminal region (P_{NTR}) and a C-terminal region (P_{CTR}) with a multimerization domain (P_{MD}) connected by a flexible linker to an NC-binding domain (P_{XD})[9,14,15] (**Fig. 1a**), and are therefore highly flexible in solution[16]. In both families, a short N-terminal region of P is sufficient to chaperone N^0 (refs. 12,13,17).

To elucidate the chaperone functions of P and to better understand the mechanism of NC assembly, we set out to reconstitute a soluble NiV N^0–P core complex and to characterize its structure in solution and in crystal. In the structure of the NiV N^0–P core complex, which to our knowledge provides the first reported nucleoprotein structure of a Paramyxovirinae, the unassembled N^0 is in an open conformation, thus providing support to the occurrence of a conformational switch between open and closed conformations and suggesting a model for NC assembly. Also, using structure-based mutagenesis, we set out to test whether interfering with the formation of the N^0–P complex can inhibit viral replication. Our results

[1]Université Grenoble Alpes, Unit of Virus Host Cell Interactions, Grenoble, France. [2]CNRS, Unit of Virus Host Cell Interactions, Grenoble, France. [3]International Centre for Research in Infectiology (CIRI), INSERM U1111–CNRS UMR5308, Université Lyon 1, Ecole Normale Supérieure de Lyon, Lyon, France. [4]Université Grenoble Alpes, Institut de Biologie Structurale, Grenoble, France. [5]CNRS, Institut de Biologie Structurale, Grenoble, France. [6]Commissariat à l'Énergie Atomique (CEA), Institut de Biologie Structurale, Grenoble, France. Correspondence should be addressed to M.J. (jamin@embl.fr) or V.V. (viktor.volchkov@inserm.fr).

Received 10 May; accepted 3 July; published online 10 August 2014; doi:10.1038/nsmb.2868

indicate that a peptide derived from P inhibits viral replication in human cells.

RESULTS

Reconstitution of a functional NiV N^0–P core complex

We reconstituted several structural variants of the NiV N^0–P complex, using peptides encompassing the N^0-binding region of P and recombinant N molecules truncated at the NT_{ARM} and the CT_{ARM} and N_{TAIL}. By size-exclusion chromatography (SEC) combined with multiangle laser light scattering (MALLS) (**Fig. 1b**) and by small-angle X-ray scattering (SAXS), we found that these reconstituted N^0–P core complexes are compact heterodimers with an overall bean-like shape typical of other NNV N proteins[18] (**Supplementary Fig. 1a–c**).

We mapped the region of P that directly interacts with N^0 by NMR spectroscopy. For this purpose, we expressed and purified a peptide of 100 amino acids (aa) corresponding to the N-terminal region of P (P_{100}) and characterized its structural properties. By SEC-MALLS, we showed that the peptide is monomeric in solution and that both its hydrodynamic radius measured by SEC and its radius of gyration measured by SAXS were larger than expected for a globular protein of this molecular mass (**Supplementary Fig. 2a,b**). In addition, the poor chemical-shift dispersion of amide resonances in the HSQC NMR spectrum was typical of disordered protein, but after assigning the NMR spectrum, the secondary-structure propensity (SSP) parameter calculated from Cα and Cβ secondary chemical shifts indicated the presence of five fluctuating α-helices (**Supplementary Fig. 2c**). We then analyzed the HSQC spectrum of P_{100} bound to $N_{32–402}$. In a complex of this size (~50 kDa), NMR signals are strongly broadened in protonated samples, thus precluding their detection, but in the HSQC spectrum we observed resonances corresponding to residues 50 to 100, thus indicating that this region remains flexible in the complex and that the N^0-binding region is comprised within the first 50 N-terminal amino acids of P (**Fig. 1c** and **Supplementary Fig. 1d**).

Accordingly, we demonstrated that a peptide corresponding to the first 40 residues of P (P_{40}) is sufficient to maintain N in a soluble form *in cellula* (**Fig. 1d**). In human cells expressing NiV N alone, we observed a punctuate distribution that can be attributed to the inherent self-assembly properties of the protein. In cells coexpressing both N and GFP-fused P_{40}, we observed a notably homogenous distribution of N in the cell and colocalization of N with P_{40}, suggesting that the N^0–P_{40} complex forms in the intracellular environment and leads to the solubilization of N (**Fig. 1d**).

Crystal structure of the NiV N^0–P core complex

The NiV $N_{32–383}{}^0$–P_{50} complex crystallized in space group $P2_12_12_1$ with three heterodimers in the asymmetric unit (**Supplementary Fig. 3**). We determined the structure at 2.5-Å resolution by the single-wavelength anomalous dispersion (SAD) method (**Fig. 1e** and **Table 1**). NiV N exhibited the two-domain structure characteristic of NNV N (refs. 5–8), defining a basic groove that can bind RNA (**Supplementary Fig. 1e**). Despite the overall low sequence conservation, the N core could be divided into four different parts, N_{NTD1}, N_{NTD2}, N_{NTD3} and N_{CTD}, of which three appear to have a conserved fold among different NNV families (**Fig. 2a** and **Supplementary Fig. 4a–d**)[5–7,19]. On the basis of their localization in the structure, we defined ten motifs conserved among most members of the Paramyxovirinae and assigned them structural or functional roles (**Supplementary Tables 1** and **2**).

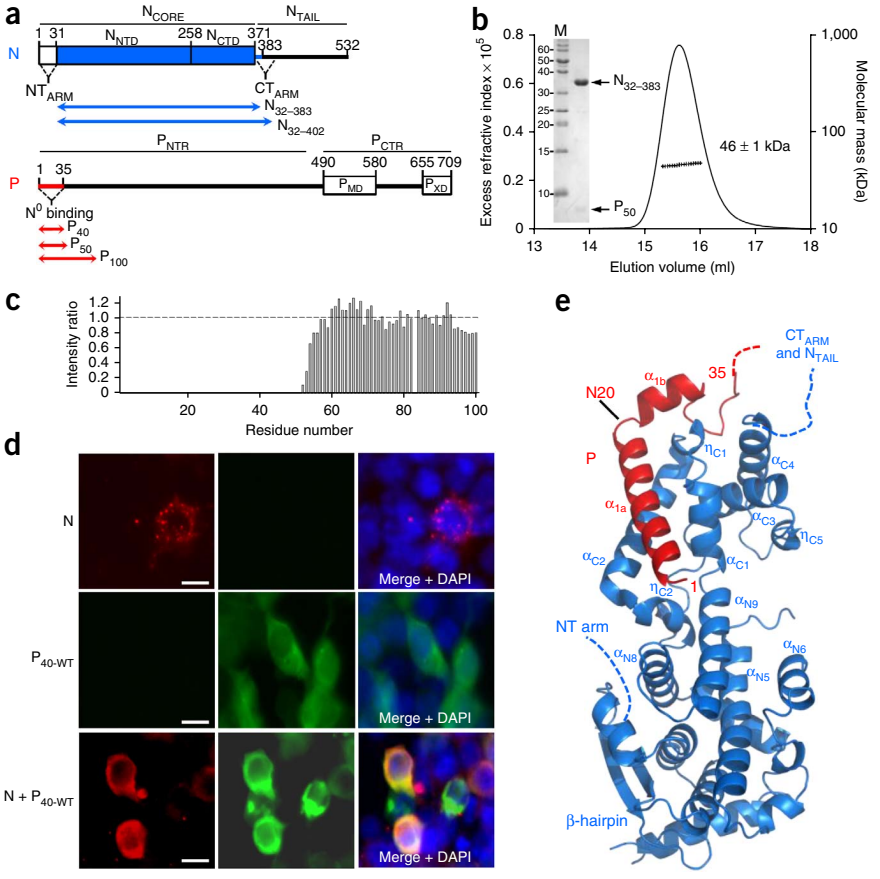

Figure 1 Structure of reconstituted NiV N^0–P complex in solution and in crystal. (**a**) Schematic architecture of NiV N and P proteins. N_{NTD}, N-terminal domain of N core; N_{CTD}, C-terminal domain of N core; NT_{ARM}, N-terminal arm of N; CT_{ARM}, C-terminal arm of N; P_{NTR}, N-terminal region of P; P_{CTR}, C-terminal region of P; P_{MD}, multimerization domain of P; P_{XD}, C-terminal X domain of P. Boxes and lines show structured domains and intrinsically disordered regions, respectively. Arrows show the recombinant constructs used in this work. (**b**) Data from SEC combined with on-line detection by MALLS and refractometry. Inset, Coomassie blue–stained SDS-PAGE gel; M, molecular mass markers (kDa). The theoretical molecular mass calculated for a heterodimeric complex is 45,613 Da. (**c**) Difference intensity profile of ^1H-^{15}N HSQC spectra of ^{15}N-labeled P_{100} in isolation and in complex with N^0. (**d**) Fluorescence microscopy images of transfected HEK293T cells expressing NiV N (red), $P_{40\text{-WT}}$ wild-type peptide in fusion with GFP (green) or both proteins (bottom row). The specificity of the anti-N antibody was demonstrated by western blot (**Supplementary Fig. 1f**). Images are representative of one of three independent experiments. Scale bars, 10 µm. (**e**) View of the crystal structure of NiV $N_{32–283}{}^0$–P_{50} in cartoon representation. $N_{32–283}{}^0$ is shown in blue and P_{50} in red. The locations of some secondary-structure elements and regions of N, as well as the C- and N-terminal residues of the P fragment, are indicated.

© 2014 Nature America, Inc. All rights reserved.

Table 1 Data collection and refinement statistics

	$N_{32–383}{}^0–P_{50}$ (SeMet)
Data collection[a]	
Space group	$P2_12_12_1$
Cell dimensions	
a, *b*, *c* (Å)	82.9, 99.0, 156.9
Resolution (Å)	49.4–2.5 (2.65–2.50)[b]
R_{merge} (%)	7.9 (46.4)
$I / \sigma I$	10.5 (2.1)
Completeness (%)	99.3 (97.9)
Redundancy	3.8 (3.9)
Refinement	
Resolution (Å)	47.2–2.5 (2.55–2.50)
No. reflections	45,315 (2,670)
R_{work} / R_{free} (%)	19.2 (24.9) / 25.9 (33.4)
No. atoms	
Protein	7,542
Ligand/ion	9
Water	99
B factors	
Protein	62.0
Ligand/ion	49.3
Water	46.7
r.m.s. deviations	
Bond lengths (Å)	0.01
Bond angles (°)	1.15

[a]Data collection statistics are calculated for unmerged Friedel pairs. [b]Values in parentheses are for highest-resolution shell. SeMet, selenomethionine.

The N-terminal chaperone region of P is stabilized upon binding to its N^0 partner, but only the first 35 residues of P, corresponding to the first fluctuating helix observed in solution (helix α_{P1}), were visible in the crystal structure of $N_{32–383}{}^0–P_{50}$. In the complex, this region formed a 2.9-nm-long helix (helix α_{P1a}; aa 1–19) with a 90° kink at residue N20 leading to a short helix (helix α_{P1b}; aa 21–28) (**Fig. 1e** and **Supplementary Fig. 2c**). The long helix α_{P1a} docks to a shallow hydrophobic groove of N_{CTD} formed by helices α_{C1}, η_{C1} and α_{C2} of conserved motif 6 (aa 265–305), and the short helix docks to the top of N_{CTD} (motif 10) (**Fig. 1e**). The complex involves multiple hydrophobic contacts and eight hydrogen bonds for a total surface area buried in the interaction of 1,440 Å^2.

NiV N is in an open conformation in N^0–P complex

By comparing the structure of NiV $N_{32–383}{}^0–P_{50}$ with that of RSV N in complex with RNA[5], we found that the fold of N is conserved (**Fig. 2a** and **Supplementary Fig. 4**) but that the putative RNA-binding groove of NiV N^0 is open, with N_{NTD} bowing down by about 30° from the N_{CTD} (**Fig. 2b**). We observed that a tyrosine residue (Y337), an aspartate residue (D175) and four out of the five basic residues (K170, R184, R185, R338 and R342) interacting with RNA in RSV N (**Fig. 2c**) are present at equivalent positions (Y354, D184 and K178, R192, R193 and R352, respectively) in the helix α_{N5}, the α_{N5}-α_{N6} loop, the helix α_{N6} and the α_{C3}-α_{C4} loop of NiV N (**Fig. 2d**) and are conserved among Paramyxovirinae. However, they are too far apart in NiV N^0 to concurrently interact with an RNA molecule. Independent three-dimensional alignments of NiV N_{NTD} and N_{CTD} with RSV N brought these residues into similar positions in both proteins (**Fig. 2b**,**d**), thus suggesting a common mechanism of conformational switching between open and closed conformations that involves a hinge motion between N_{CTD} and N_{NTD}, in agreement with normal-mode simulations (**Supplementary Fig. 5a–c** and **Supplementary Movie 1**).

RNA binding and the rule of six

In RSV NCs, each N interacts with 7 nt, and base 1 packs on the flat surface of helix α_{N9} formed by two glycine residues (G241 and G245) (**Fig. 2e** and **Supplementary Fig. 5d**)[5]. However, in the

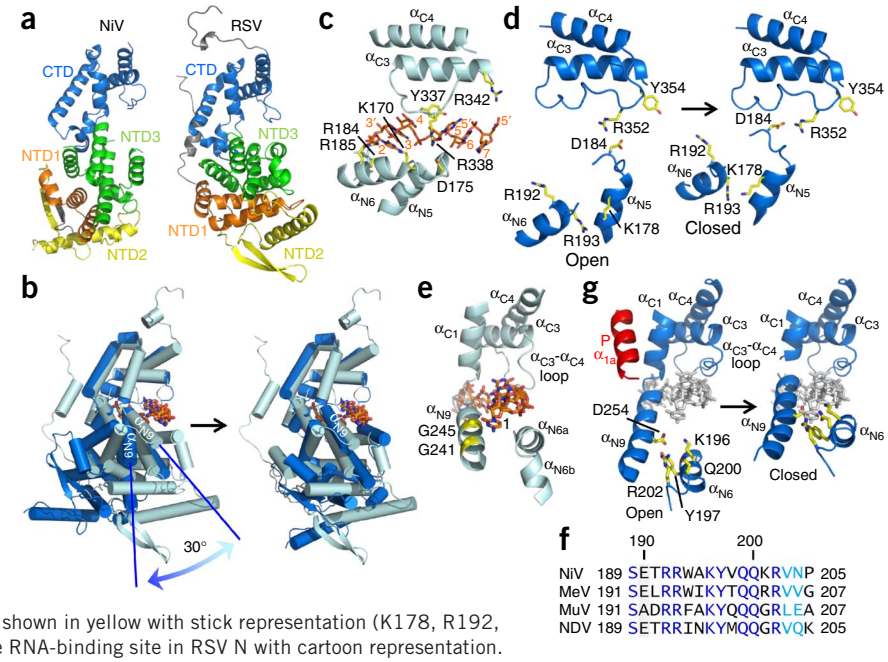

Figure 2 Comparison of NiV and RSV N proteins reveals an open-to-closed conformational change. (**a**) View of the structures of NiV N and RSV N (PDB 2WJ8 (ref. 5)) in similar orientations. Corresponding domains and subdomains are colored in the same color code. (**b**) Structural comparisons of NiV $N_{32–383}$ in its crystal structure (left) and in a hypothetical closed conformation (right) with RSV N taken from the NC-like complex (PDB 2WJ8 (ref. 5)). Dark blue, NiV $N_{32–383}$; light blue, RSV N; orange, RNA bound to RSV N. The lines at left show the direction of the α_{N9} axis in each protein. The hypothetical closed form of NiV N was obtained by independently aligning NiV N_{NTD} and N_{CTD} on the corresponding domains of RSV N. (**c**) Front view of the RNA-binding site in RSV N. Residues interacting with RNA and conserved in several members of the Paramyxovirinae (K170, R184, R185, R338, D175 and Y337) are shown in yellow in stick representation. (**d**) Front view of the putative RNA-binding groove of NiV N in its open and hypothetical closed conformations. The residues corresponding to those shown in **c** are shown in yellow with stick representation (K178, R192, R193, R352, D184 and Y354). (**e**) Side view of the RNA-binding site in RSV N with cartoon representation. Two glycine residues (G241 and G245) forming a flat surface on helix α_{N9} and interacting with base 1 of the 7 nt bound to each N protomer are shown in yellow. (**f**) Multiple sequence alignment of representative members of the subfamily Paramyxovirinae (**Supplementary Table 1**, motif 3). MeV, measles virus (Morbillivirus); MuV, mumps virus (Rubulavirus); NDV, Newcastle disease virus (Avulavirus). (**g**) Side view of the putative RNA-binding groove of NiV N in its open and hypothetical closed conformations. The RNA molecule (in gray) is docked against NiV N_{CTD} as in RSV NC.

© 2014 Nature America, Inc. All rights reserved.

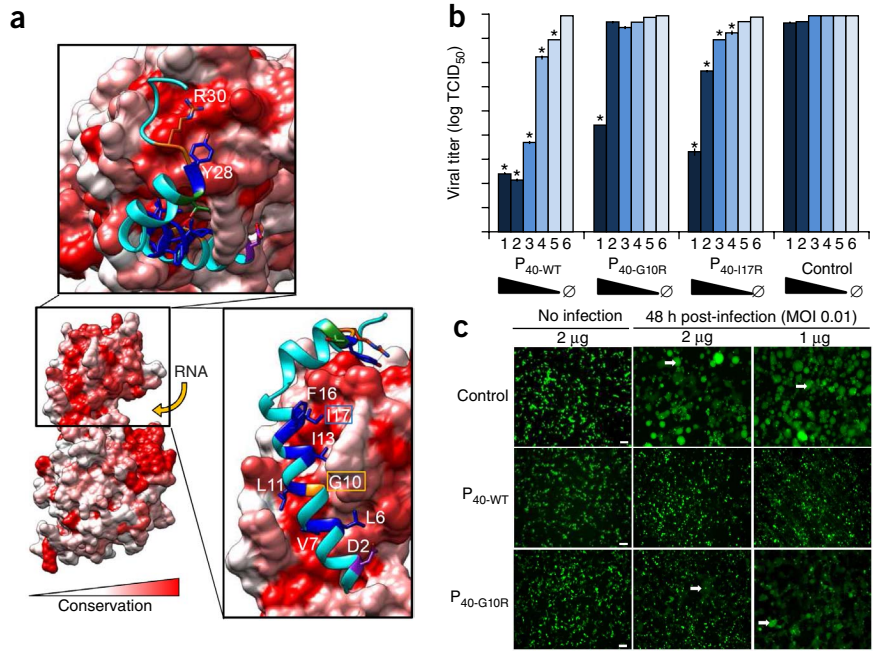

Figure 3 Conservation of the N^0-P interface and inhibition of NiV replication by the N^0-binding peptide of P. (**a**) View of the NiV $N_{32–283}{}^0$–P_{50} complex with surface and conservation representations for $N_{32–383}$ and with cartoon and stick representations for P_{50}. The conservation in N derived from multiple sequence alignment is displayed on the surface of NiV N: white, low-level conservation, <20%; red, high-level conservation, >80%. The side chains of conserved residues in the P N-terminal region are shown in stick representation. Conserved residues are colored as follows: violet, acidic; red, basic; blue, hydrophobic; green, polar; orange, glycine. (**b**) Quantification of the effect of peptide expression on viral replication. Viral titer measured 48 h after infection with NiV (multiplicity of infection (MOI), 0.01) in culture supernatant of HEK293T cells transfected with varying amounts (bars 1–5, 2 µg to 0.125 µg; Ø, absence of plasmid) of plasmids coding for GFP alone (control), $P_{40\text{-}WT}$, $P_{40\text{-}G10R}$ or $P_{40\text{-}I17R}$ ($n = 6$ cell culture replicates) $^*P < 0.05$ by one-way ANOVA test. $TCID_{50}$, median tissue culture–infective dose. (**c**) Syncytia formation in NiV-infected cells expressing GFP (control) or GFP-$P_{40\text{-}WT}$ or GFP-$P_{40\text{-}G10R}$. White arrows show examples of typical syncytia formation. Images are representative of three independent experiments. Scale bars, 50 µm.

Paramyxovirinae subfamily, N binds to only 6 nt, and the genome obeys a rule of six; i.e., there is a strict requirement for their genome to consist of a multiple of 6 nt (refs. 20,21). In the putative closed form of NiV N, we found that several residues in helix α_{N6} (conserved motif 3) (**Fig. 2f**) and D254 in helix α_{N9} (conserved motif 5) hinder a similar packing of base 1 (**Fig. 2g** and **Supplementary Fig. 5e**). The presence of motif 3, which is strictly conserved in the Paramyxovirinae subfamily but is absent in the Pneumovirinae subfamily, might thus explain why the N protein of the Paramyxovirinae binds only 6 nt and why these viruses obey the rule of six.

Conservation of the N^0-P binding interface

NNV P proteins vary greatly in length and sequence[22], with sequence conservation generally becoming undetectable beyond the family level. However, a recent study identified residues in the N-terminal region of P that are conserved among most members of the Paramyxoviridae in spite of an overall distant evolutionary relationship[23]. Most of these conserved residues appeared to be key residues for the interaction with N^0 (**Fig. 3a** and **Supplementary Fig. 2d**), whereas mapping residue conservation among Paramyxovirinae onto the surface of NiV N reveals a strong conservation of the binding site for P_{NTR} (**Fig. 3a**). These results thus suggest a conserved structural architecture of the N^0–P complex among different genera of the subfamily.

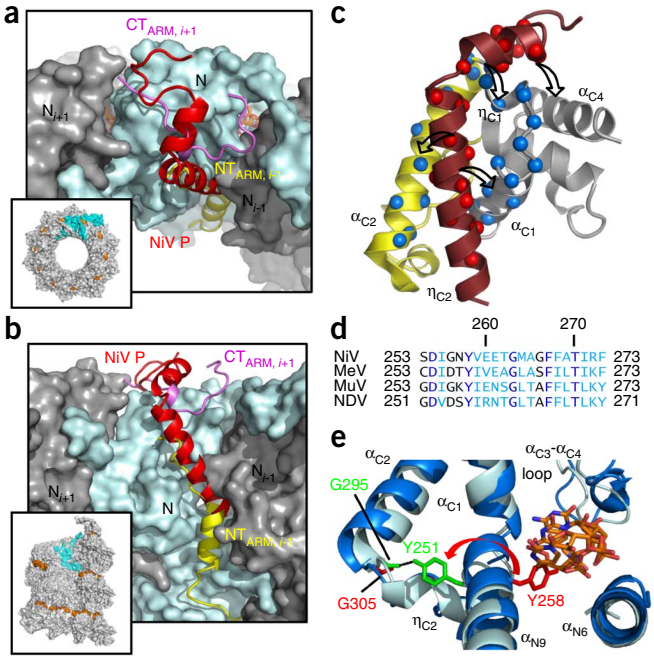

Figure 4 Chaperone activities of NiV P. (**a**) Top view of one RSV N protomer within the N–RNA complex shown with surface representation for N_{CORE} (in light blue) (PDB 2WJ8 and 4BKK (ref. 5)) aligned with N_{CTD} of NiV $N_{32–283}{}^0$–P_{50} complex. The NT_{ARM} of the N_{i-1} RSV N protomer (in yellow) and the CT_{ARM} of the N_{i+1} RSV N protomer (in violet) are shown with cartoon representation. Only P_{50} of the NiV complex is shown (in red, cartoon representation). The inset shows the localization of the RSV N protomer within the NC. (**b**) Front view of the same structural overlay. The inset shows the localization of RSV N protomer within the NC. (**c**) View of NiV P_{50} bound to N_{CTD} in the $N_{32–283}{}^0$–P_{50} complex with cartoon representation. Dark red, P_{50}; yellow, latch in N_{CTD}; red and blue spheres, C_α of residues making contacts between P_{50} and N_{CTD} ($N_{32–283}{}^0$), respectively. Arrows indicate the connections between P_{50} and the helices α_{C1}, η_{C1}, α_{C2} and α_{C4} of N_{CTD}. (**d**) Multiple sequence alignment of representative members of the subfamily Paramyxovirinae (**Supplementary Table 1**, motif 6). (**e**) Structural overlay of RSV N–RNA complex in light blue and NiV $N_{32–383}$ in the putative closed conformation in dark blue, with cartoon representation. Residues Y258 and G305 of NiV N (in red) and residues Y251 and G295 of RSV N (in green) are shown with stick representation. The red arrow indicates the hypothetical rotation of Y258 upon P release.

© 2014 Nature America, Inc. All rights reserved.

Inhibition of NiV replication

We found that expression of GFP-fused P_{40} peptide in human cells (HEK293T) before infection significantly inhibits viral growth in a dose-dependent manner and abolishes syncytium formation, the latter being a hallmark of NiV infection (**Fig. 3b**,**c**). We used the $N_{32–383}{}^0$–P_{50} crystal structure to design peptide variants that destabilize the interface between N^0 and P_{50} and found that the variants in which conserved residues G10 or I17 (ref. 23) are mutated to arginine (G10R or I17R) were less efficient in inhibiting viral replication. These results thus confirmed the specificity of the interaction observed in the crystal and in solution (**Fig. 3b**,**c**). Because the reconstituted N^0–P core complex lacks a large part of the P molecule, notably the tetramerization domain and both polymerase- and NC-binding regions, we hypothesize that P_{40} might inhibit viral growth by trapping N^0 in a nonproductive complex.

The chaperone functions of P

To understand the chaperone functions of P_{NTR}, we used RSV N–RNA complex as a model for the NiV N–RNA complex (**Fig. 4a**,**b**). When we aligned the N_{CTD} of NiV $N_{32–383}{}^0$–P_{50} with the N_{CTD} of one N protomer of the RSV N–RNA complex, we found that helix α_{P1b} competes with the CT_{ARM} of the N_{i+1} protomer for the same binding site on the N surface (**Fig. 4a**), whereas helix α_{P1a} competes with the NT_{ARM} of the N_{i-1} protomer (**Fig. 4b**). A first role of P is thus to prevent the polymerization of N by interfering with the binding of exchanged subdomains. The structure of the NiV $N_{32–383}{}^0$–P_{50} complex also suggested that bound P prevents NC assembly and RNA binding by trapping N^0 in an open conformation without directly interfering with RNA (**Fig. 2g**). The closure of the molecule requires that helices α_{N5} and α_{N9} rotate around pivots near the N_{NTD}-N_{CTD} junction (**Fig. 2b**). Helices α_{C2}, η_{C2}, η_{C3} and η_{C4} form a latch with helices η_{C2} and η_{C3} docked against the C-terminal end of helices α_{N5} and α_{N9}. Motions of helices α_{N5} and α_{N9} thus require that the latch move away from the N_{CTD} core. We propose that by bridging helices α_{C1}, η_{C1}, α_{C2} and α_{C4} (**Fig. 4c**), P rigidifies the entire N_{CTD} domain and prevents global conformational changes in N. In addition, the bulky side chain of Y258, a highly conserved residue among Paramyxoviridae (**Fig. 4d**), points inside the RNA-binding groove, thus preventing the RNA from coming into contact with the surface of the protein (**Fig. 4e**). In the RSV N–RNA complex, Y251, similarly located at the end of helix α_{N9}, points in the opposite direction and docks against the backbone of a glycine residue in helix α_{C2}. A glycine is also conserved (motif 6, **Supplementary Table 1**) at this position in NiV N, thus suggesting that the tyrosine side chain flips away upon RNA binding (**Fig. 4e**), but in the N^0–P complex, motion of Y258 is hindered by the presence of the N-terminal end of P. Alternatively, Y258 might interact with one of the RNA bases.

DISCUSSION

We present here the structure of the N^0–P core complex of Nipah virus, in which unassembled N^0 is maintained in an open conformation by a short N-terminal region of P_{NTR}. These results unveil the mechanism of P chaperone activities and provide experimental evidence that NNV N switches between open and closed conformations during NC assembly. The comparison with the recent structure of the N^0–P core complex of VSV[17], in the Rhabdoviridae family, reveals a common feature in the mechanism of N^0 chaperoning by P. In both cases, the N-terminal N^0-binding region of P_{NTR} prevents N polymerization by occupying the binding cavity for arms, NT_{ARM} and CT_{ARM}, of adjacent N molecules. It also reveals major differences. First, the part of P_{NTR} that directly blocks the exchange of N arms has a different length and adopts a different structure; in the VSV complex, only a short part of P_{NTR} (aa 7–14) binds in an extended conformation into the N arm–binding cavity, whereas in the NiV complex, the entire length of the P_{NTR} N^0-binding region, forming helices αP_{1A} and αP_{1B} (aa 1–35), occupies the N arm–binding sites. Also, the NiV P_{NTR} binds to the surface of N_{CTD} in the opposite direction as compared with the NT_{ARM} of the Ni-1 protomer in the polymeric N-RNA complex. Second, NiV P_{NTR} binds exclusively to N_{CTD}, not directly interfering with RNA binding, whereas a part of VSV P_{NTR} forms a helix (aa 15–35), which binds at the interface of N_{NTD} and N_{CTD} and protrudes in the RNA-binding groove. Third, NiV N^0 is in an open conformation, and we propose here that by bridging secondary-structure elements

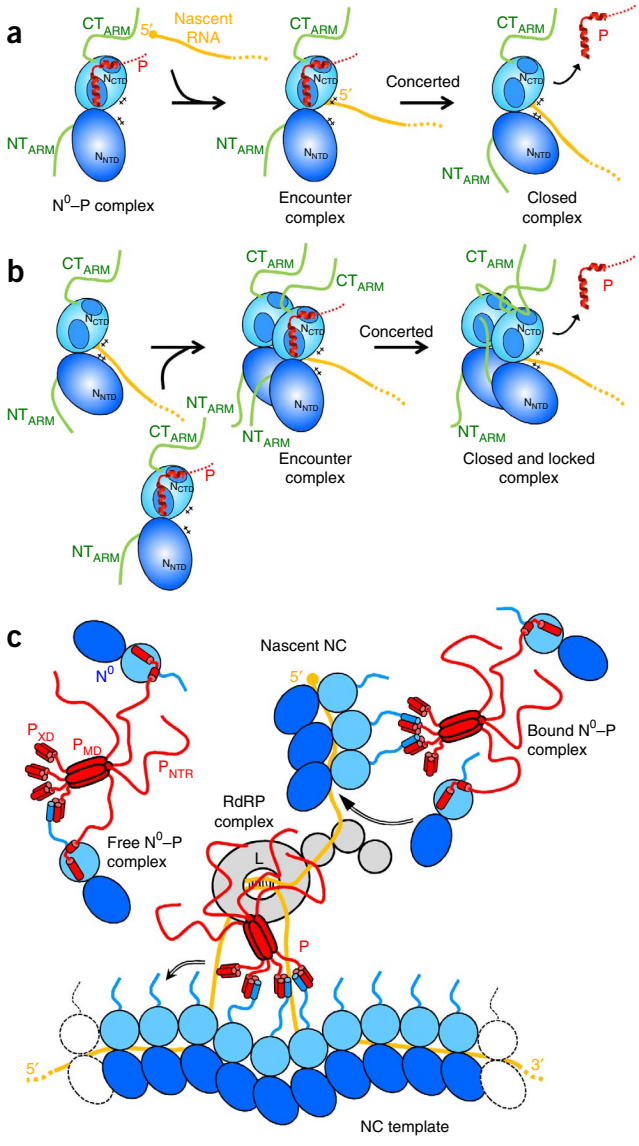

Figure 5 Proposed mechanism for RNA encapsidation in the Paramyxovirinae subfamily. (**a**) Binding of the first N protomer. Red, P_{50}; orange, genomic RNA; light blue, N_{NTD}, with dark-blue circles indicating binding sites for the exchanged subdomains; dark blue, N_{CTD}; green, NT_{ARM} and CT_{ARM}-N_{TAIL}. (**b**) Assembly of the N protomers. (**c**) Scheme of the RNA transcription-replication complex. The NT_{ARM} has been omitted for the sake of clarity, and the CT_{ARM}-N_{TAIL} is shown in blue. The RNA-dependent RNA polymerase (RdRP) is shown in gray. The N^0–P complex formed with tetrameric P is shown in a hypothetical complex with NC, involving the interaction between P_{XD} and N_{TAIL}.

© 2014 Nature America, Inc. All rights reserved.

in N_{CTD}, P_{NTR} hinders closure of the molecule and prevents RNA encapsidation. By contrast, in the VSV N^0–P core complex, N^0 is in the same closed conformation as it is in the N–RNA complex[17]. The *a posteriori* analysis of the VSV N^0–P core structure suggests, however, that P_{NTR} bridges N_{NTD} and N_{CTD} in the closed conformation, preventing the opening of the molecule that is necessary to accommodate the RNA molecule and unveiling another common feature of both systems, namely the blocking of the conformational switch by hindering domain motions.

On the basis of the structure reported here, we propose a possible scenario for the assembly of Paramyxovirinae N^0 molecules along newly synthesized viral RNA, via a concerted mechanism of transfer of N^0 from the N^0–P complex to the nascent RNA molecule, which involves the release of P and the closure of the RNA-binding groove (**Fig. 5a**,**b**). Although the mechanism by which the initial N^0 is recruited to the 5′ end of nascent RNA remains to be determined, we assume that, in a first step, the encounter complex forms with the RNA molecule loosely inserted in the open cavity. Then, in a second concerted step, P is released, and N grasps the RNA molecule (**Fig. 5a**). The release of P from the RNA-bound N frees the binding site for the NT_{ARM} of the next incoming N molecule. Upon formation of the encounter complex with the next N^0–P complex, the NT_{ARM} of the incoming N can bind to the previously bound N. The CT_{ARM} of bound N can also bind to the incoming N and can help displace the P peptide (**Fig. 5b**). In a second or concomitant process, P is released, and N closes onto the RNA. The NT_{ARM} of the second bound N molecule locks the first N in its closed conformation by bridging N_{NTD} with N_{CTD} (**Fig. 5b**).

We confirmed that the short N^0-binding region of P is sufficient to chaperone N^0 and to keep it in a soluble form, but we also found that P_{40} inhibited viral replication, thus indicating that the N-terminal region of P is not sufficient to enable NC assembly and suggesting the involvement of other regions of P in this process. P is a multifunctional, highly flexible molecule, which also possesses binding sites for L or for NCs, and it is thus plausible that interactions with these other viral proteins are necessary to correctly position the N^0–P complex at the site of viral RNA synthesis (**Fig. 5c**). The attachment of N^0–P to the NC (as suggested in **Fig. 5c**) would raise the local concentration around the site of RNA synthesis and thereby favor the encapsidation of the viral RNA genome.

The successful inhibition of NiV infection by the N^0-binding peptide of P suggests that the P-binding cavity in N can be specifically targeted for designing inhibitors of NiV replication. The structure of the N^0–P core complex provides the structural basis for designing small molecules or peptidomimetics that could prevent the formation of the complex. The strong conservation of the binding interface suggests that NiV $N_{32-383}{}^0$–P_{50} structure is a good structural model for the N^0–P complex of other paramyxoviruses and that possibly a broad-spectrum drug might be developed against several viruses.

METHODS

Methods and any associated references are available in the online version of the paper.

Accession codes. Coordinates and structure factors have been deposited in the Protein Data Bank under accession code 4CO6.

Note: Any Supplementary Information and Source Data files are available in the online version of the paper.

ACKNOWLEDGMENTS

We thank W. Burmeister and A. McCarthy for their help with X-ray data collection and C. Leyrat for discussions. F.Y. was supported by a predoctoral fellowship from the Région Rhône-Alpes. This work was supported by grants from the French Agence Nationale de la Recherche to M.J. (ANR-07-001-01) and to V.V. (ANR-09-MIEN-018-01), from the European Commission's FP7 program ANTIGONE (278976) to V.V. and from the Fondation Innovations en Infectiologie (FINOVI) to V.V. and M.J. This work used the platforms of the Grenoble Instruct center (Integrated Structural Biology Grenoble; UMS3518 CNRS-CEA-UJF-EMBL) with support from The French Infrastructure for Integrated Structural Biology (FRISBI) (ANR-10-INSB-05-02) and The Alliance Grenobloise pour la Biologie Structurale et Cellulaire Intégrées (GRAL) (ANR-10-LABX-49-01) within the Grenoble Partnership for Structural Biology (PSB).

AUTHOR CONTRIBUTIONS

F.Y., P.L., M.R.J., R.W.H.R., M.B., V.V. and M.J. designed all experiments. F.Y., P.L., E.D. and M.R.J. performed the experiments. P.L. performed BSL-4 experiments. F.Y., P.L., N.T., J.-M.B., M.R.J., R.W.H.R., M.B., V.V. and M.J. contributed to data analysis. F.Y., P.L., M.R.J., M.B., V.V. and M.J. wrote the paper.

COMPETING FINANCIAL INTERESTS

The authors declare no competing financial interests.

Reprints and permissions information is available online at http://www.nature.com/reprints/index.html.

1. Pringle, C.R. The order Mononegavirales: current status. *Arch. Virol.* **142**, 2321–2326 (1997).
2. Chua, K.B. *et al.* Nipah virus: a recently emergent deadly paramyxovirus. *Science* **288**, 1432–1435 (2000).
3. Morin, B., Rahmeh, A.A. & Whelan, S.P. Mechanism of RNA synthesis initiation by the vesicular stomatitis virus polymerase. *EMBO J.* **31**, 1320–1329 (2012).
4. Arnheiter, H., Davis, N.L., Wertz, G., Schubert, M. & Lazzarini, R.A. Role of the nucleocapsid protein in regulating vesicular stomatitis virus RNA synthesis. *Cell* **41**, 259–267 (1985).
5. Tawar, R.G. *et al.* Crystal structure of a nucleocapsid-like nucleoprotein-RNA complex of respiratory syncytial virus. *Science* **326**, 1279–1283 (2009).
6. Albertini, A.A. *et al.* Crystal structure of the rabies virus nucleoprotein-RNA complex. *Science* **313**, 360–363 (2006).
7. Green, T.J., Zhang, X., Wertz, G.W. & Luo, M. Structure of the vesicular stomatitis virus nucleoprotein-RNA complex. *Science* **313**, 357–360 (2006).
8. Desfosses, A., Goret, G., Estrozi, L.F., Ruigrok, R.W. & Gutsche, I. Nucleoprotein-RNA orientation in the measles virus nucleocapsid by three-dimensional electron microscopy. *J. Virol.* **85**, 1391–1395 (2011).
9. Karlin, D., Ferron, F., Canard, B. & Longhi, S. Structural disorder and modular organization in *Paramyxovirinae* N and P. *J. Gen. Virol.* **84**, 3239–3252 (2003).
10. Jensen, M.R. *et al.* Intrinsic disorder in measles virus nucleocapsids. *Proc. Natl. Acad. Sci. USA* **108**, 9839–9844 (2011).
11. Communie, G. *et al.* Atomic resolution description of the interaction between the nucleoprotein and phosphoprotein of Hendra virus. *PLoS Pathog.* **9**, e1003631 (2013).
12. Curran, J., Marq, J.B. & Kolakofsky, D. An N-terminal domain of the Sendai paramyxovirus P protein acts as a chaperone for the NP protein during the nascent chain assembly step of genome replication. *J. Virol.* **69**, 849–855 (1995).
13. Mavrakis, M. *et al.* Rabies virus chaperone: identification of the phosphoprotein peptide that keeps nucleoprotein soluble and free from non-specific RNA. *Virology* **349**, 422–429 (2006).
14. Gérard, F.C.A. *et al.* Modular organization of rabies virus phosphoprotein. *J. Mol. Biol.* **388**, 978–996 (2009).
15. Habchi, J., Mamelli, L., Darbon, H. & Longhi, S. Structural disorder within Henipavirus nucleoprotein and phosphoprotein: from predictions to experimental assessment. *PLoS ONE* **5**, e11684 (2010).
16. Leyrat, C. *et al.* Ensemble structure of the modular and flexible full-length vesicular stomatitis virus phosphoprotein. *J. Mol. Biol.* **423**, 182–197 (2012).
17. Leyrat, C. *et al.* Structure of the vesicular stomatitis virus N-P complex. *PLoS Pathog.* **7**, e1002248 (2011).
18. Ruigrok, R.W., Crepin, T. & Kolakofsky, D. Nucleoproteins and nucleocapsids of negative-strand RNA viruses. *Curr. Opin. Microbiol.* **14**, 504–510 (2011).
19. Rudolph, M.G. *et al.* Crystal structure of the Borna disease virus nucleoprotein. *Structure* **11**, 1219–1226 (2003).
20. Calain, P. & Roux, L. The rule of six, a basic feature for efficient replication of Sendai virus defective interfering RNA. *J. Virol.* **67**, 4822–4830 (1993).
21. Halpin, K., Bankamp, B., Harcourt, B.H., Bellini, W.J. & Rota, P.A. Nipah virus conforms to the rule of six in a minigenome replication assay. *J. Gen. Virol.* **85**, 701–707 (2004).
22. Lamb, R.A. in *Fields Virology* 6th edn, Vol. 1 (eds. Knipe, D.M. & Howley, P.M.) 880–884 (Lippincott Williams & Wilkins, Philadelphia, 2013).
23. Karlin, D. & Belshaw, R. Detecting remote sequence homology in disordered proteins: discovery of conserved motifs in the N-termini of *Mononegavirales* phosphoproteins. *PLoS ONE* **7**, e31719 (2012).

© 2014 Nature America, Inc. All rights reserved.
npg

ONLINE METHODS

Multiple sequence alignment. Multiple sequence alignment with MAFFT[24] was performed for N proteins in the Paramyxovirinae subfamily (not including Respiroviruses) with the following sequences: NiV, Nipah virus, UMMC1 isolate, UniProt Q9IK92; HeV, Hendra virus, UniProt O89339; CeV, Cedar virus, UniProt J7H328; MeV, Measles virus, UniProt P04851; CDV, Canine distemper virus, UniProt P04865; DMV, Dolphin morbillivirus, UniProt Q66412; PPRV, Peste des petits ruminants, UniProt Q08823; RPV, Rinderpest virus, UniProt Q03332; MuV, Mumps virus, UniProt Q77IS8; HPIV2, Human parainfluenza virus 2, UniProt P21737; HPIV4a, Human parainfluenza virus 4a, UniProt P17240; MPV, Mapuera virus, UniProt A5H724; MNV, Menangle virus, UniProt K9N0Q8; SV41, Simian virus 41, UniProt P27018; SV5, Simian virus 5, UniProt Q88435, NDV, Newcastle disease virus, UniProt Q99FY3; AMPV2, Avian paramyxovirus 2, UniProt F5BH21; AMPV3, Avian paramyxovirus 3, UniProt D5FGX2; and AMPV4, Avian paramyxovirus 4, UniProt B5AXP0.

Reconstitution of the N^0–P core complex. Constructs comprising residues 1–50 (P_{50}) of P and residues 32–383 ($N_{32–383}$) or 32–402 of N ($N_{32–402}$) from the Malaysian isolate UMMC1 of Nipah virus (UniProt Q9IK91 and Q9IK92) were cloned in the pETM40 vector in fusion with an N-terminal maltose-binding protein (MBP) tag. All proteins were expressed in *Escherichia coli* BL21 (DE3) Rosetta cells. Cells were grown at 37 °C in LB medium until the OD reached 0.6, and protein expression was induced overnight at 20 °C by addition of isopropyl-β-D-thiogalactoside (IPTG) to a final concentration of 1 mM. Cells were harvested, and the pellet was suspended in buffer A for the P construct (20 mM Tris-HCl buffer at pH 7.5 containing 150 mM NaCl, 50 mM arginine, 50 mM glutamate and 0.5 mM Tris(2-carboxyethyl)phosphine (TCEP)) and in buffer B for N constructs (Tris-HCl buffer at pH 7.5 containing 150 mM NaCl). All buffers were supplemented with Complete protease inhibitor cocktail (Roche). Cells were disrupted by sonication, and the crude extract was cleared by centrifugation at 45,000*g* at 4 °C for 20 min. The supernatant was loaded onto an amylose resin column (New England BioLabs) equilibrated in buffer A or B. The column was washed with ten volumes of buffer A or B containing 500 mM NaCl, and the protein was eluted with 50 mM maltose (Sigma) in buffer A or B.

The P-MBP fusion protein was cleaved with TEV protease to remove the MBP tag. The protease was added at an approximate weight ratio of 100:1 (fusion protein/TEV), and digest was performed in buffer A overnight at 4 °C. After concentration with Vivaspin concentrators (GE Healthcare) with a 3-kDa cutoff, the protein solution was loaded onto a S75 Superdex (GE Healthcare) column equilibrated in buffer A at 4 °C. The purified P peptide was mixed with purified N-MBP, and the mixture was incubated overnight at 4 °C. After concentration, the solution was loaded onto a S75 Superdex column equilibrated in buffer A. The fractions containing the N^0–MBP-P complex were pooled, and the MBP tag was cleaved by incubation overnight at 4 °C in the presence of TEV protease at a weight ratio of 100:1. The solution was concentrated and loaded onto a S75 Superdex (GE Healthcare) column coupled to a short amylose resin (NEB) column equilibrated in buffer B to completely remove cleaved MBP. The fractions containing the N^0–P complex were pooled and concentrated with Amicon concentrators (Millipore) with a 10-kDa cutoff. During the purification process, protein purity was checked by SDS-PAGE.

A construct comprising residues 1–100 (P_{100}) of P was cloned in the pET28 vector with a C-terminal histidine tag and expressed in *E. coli* BL21 (DE3) Rosetta cells. To produce unlabeled P_{100}, cells were grown at 37 °C in LB medium until the OD reached 0.6, and protein expression was induced overnight at 20 °C by addition of isopropyl-β-D-thiogalactoside (IPTG) to a final concentration of 1 mM. For the ^{13}C-^{15}N–labeled P_{100}, cells were grown in M9 minimal medium supplemented with MEM vitamins (Gibco), with 1.0 g L^{-1} of $^{15}NH_4Cl$ and 4.0 g L^{-1} of ^{13}C glucose as previously described[25]. Cells were harvested, and the pellet was suspended in buffer A (without TCEP) supplemented with Complete protease inhibitor cocktail (Roche). Cells were disrupted by sonication, and the crude extract was cleared by centrifugation at 45,000*g* at 4 °C for 20 min. The supernatant was loaded onto a His Select resin (Sigma) column preequilibrated in buffer A. The column was washed with ten volumes of buffer A containing 500 mM NaCl and 10 mM imidazole (Sigma), and the protein was eluted in buffer A containing 300 mM imidazole. The fractions containing the peptide were pooled and concentrated with Vivaspin concentrators (GE Healthcare) with a 5-kDa cutoff. The solution was loaded onto a S200 Superdex column equilibrated in buffer A at 4 °C. Fractions containing the peptide were pooled and concentrated. For NMR experiments, P_{100} was prepared and the $N_{32–402}{}^0$–P_{100} complex was reconstituted as described above, and buffer A was exchanged with 20 mM Bis-Tris buffer at pH 6.0 containing 150 mM NaCl, 50 mM arginine, 50 mM glutamate and 0.5 mM TCEP.

To produce a selenomethionine-substituted $N_{32–383}$, cells were grown at 37 °C in M9 minimal medium supplemented with MEM vitamins (Gibco), with 1.0 g L^{-1} of NH_4Cl and 2.0 g L^{-1} of glucose until the OD reached 0.6. Then the temperature was lowered to 20 °C, and the culture was supplemented with a mix of amino acids containing 100 mg lysine, 100 mg phenylalanine, 100 mg threonine, 50 mg isoleucine, 50 mg leucine, 50 mg valine and 50 mg SeMet per liter of medium and incubated for 45 min. Protein expression was induced overnight at 20 °C by addition of isopropyl-β-D-thiogalactoside (IPTG) to a final concentration of 1 mM. The SeMet derivative was purified as described above.

SEC-MALLS experiments. Size-exclusion chromatography (SEC) combined with on-line detection by multiangle laser light scattering (MALLS) and refractometry (RI) is a method for measuring the absolute molecular mass of a particle in solution that is independent of its dimensions and shape[26]. SEC was performed with a S200 Superdex column (GE Healthcare) equilibrated with 20 mM Tris-HCl buffer containing 150 mM NaCl. Separations were performed at 20 °C with a flow rate of 0.5 mL min^{-1}. MALLS detection was performed with a DAWN-HELEOS II detector (Wyatt Technology) using a laser emitting at 690 nm, and protein concentration was measured on-line by the use of differential refractive-index measurements, with an Optilab T-rEX detector (Wyatt Technology) and a refractive-index increment, dn/dc, of 0.185 mL g^{-1}. Weight-averaged molar masses (Mw) were calculated with ASTRA (Wyatt Technology). For size determination, the column was calibrated with proteins of known Stokes radius (R_S)[27].

Small-angle X-ray scattering experiments. Small-angle X-ray scattering (SAXS) data were collected at the BioSAXS beamline (BM29) of the ESRF (http://www.esrf.eu/UsersAndScience/Experiments/MX/About_our_beamlines/BM29/). The scattering from the buffer alone was measured before and after each sample measurement and was used for background subtraction with PRIMUS from the ATSAS package[28]. Scattering data were collected at different concentrations ranging from 0.3 mg mL^{-1} to 0.6 mg mL^{-1} for P_{100} and from 0.55 mg mL^{-1} to 2.4 mg mL^{-1} for the N^0–P complex. No concentration-dependent interparticle effect was observed. R_g was estimated at low Q values by the Guinier approximation. *Ab initio* low-resolution bead models of the N^0–P complex were computed from the distance distribution function P(r) (D_{max} = 10 nm) in DAMMIN[29]. 20 low-resolution models, obtained from independent reconstructions, were aligned, averaged and filtered with DAMAVER[30].

NMR spectroscopy. The spectral assignment of P_{100} of NiV P protein was obtained at 25 °C in 20 mM Bis-Tris buffer at pH 6.0 containing 150 mM NaCl, 50 mM arginine, 50 mM glutamate and 0.5 mM TCEP with a set of BEST-type triple resonance experiments[31]. The NMR experiments were acquired at a ^1H frequency of 800 MHz. A total of six experiments were acquired: HNCO, intraresidue HN(CA)CO, HN(CO)CA and intraresidue HNCA, HN(COCA)CB and intraresidue HN(CA)CB. All spectra were processed in NMRPipe[32] and analyzed in Sparky (SPARKY 3, University of California, San Francisco), and automatic assignment of spin systems was done in MARS[33] and followed by manual verification. The ^1H-^{15}N HSQC spectrum of P_{100} was compared to the spectrum of purified $N_{32–383}{}^0$–P_{100} complex. The intensity ratio of the resonances in the two spectra was used for mapping the binding site of N^0 on P_{100}. Chemical shifts depend on the backbone ϕ and ψ dihedral angles, and in disordered systems they are highly sensitive to the presence of transient secondary structure, commonly expressed in terms of a secondary structure propensity (SSP)[34,35]. The SSP score for isolated P_{100} revealed the presence of several fluctuating α-helices (**Supplementary Fig. 2c**).

Crystallography. We used different constructs of N and P to reconstitute N^0–P analogs, but only the $N_{32–383}{}^0$–P_{50} complex crystallized. Initial crystallization conditions for the $N_{32–383}{}^0$–P_{50} complex were identified at the High Throughput Crystallization Laboratory of the EMBL Grenoble Outstation (https://htxlab.embl.fr/). Plate clusters obtained in 22% PEG 3350 and 0.2M KBr (**Supplementary Fig. 3**) were used to grow crystals of the selenomethionine derivative of the $N_{32–383}{}^0$–P_{50}

© 2014 Nature America, Inc. All rights reserved.

doi:10.1038/nsmb.2868

complex by the microseeding method. A plate cluster of native protein was crushed in 50 µl of stabilization solution (20 mM Tris-HCl at pH 8 containing 22% PEG 3350, 0.2 M KBr and 0.2 M NaCl) with the Seed Bead kit (Hampton Research). The seed stock was serially diluted (5, 25, 100 and 1,000 times), and the drops were set by mixture of 0.5 µl of the resulting seed stock, 1 µl of protein solution and 1 µl of precipitant solution. The crystals used for data collection were obtained with protein concentrations of 10 to 20 mg mL^{-1} in the presence of 16–18% PEG 3350 and 0.2 M KBr (**Supplementary Fig. 3**) and were frozen with 15% glycerol as cryoprotectant. X-ray diffraction data were collected at the ID29 beamline of the ESRF at a wavelength of 0.9793 Å and at a temperature of 100 K and were processed with the XDS package[36]. Initial phases were obtained with the anomalous scattering from selenium atoms by the SAD method, with HKL2MAP[37] (**Supplementary Fig. 3**). A model was initially constructed with Autobuild[38] from the Phenix suite[39] and subsequently refined with phenix.refine[40] and Coot[41]. 2,288 reflections were used to calculate the R_{free} parameter. The geometry of the final model was checked with MolProbity[42]. In the model, 97.0% of residues have backbone dihedral angles in the favored region of the Ramachandran plot, 2.77% fall in the allowed regions, and 0.23% are outliers. Part of the α_{N5}-α_{N6} loop is not visible in the crystal electron density. Figures have been generated with PyMOL (http://www.pymol.org/) and Chimera[43]. Low-frequency normal modes of N^0 were computed with the Elastic Network Model[44].

Plasmid construction. The sequence corresponding to residues 1–40 of NiV P was cloned in frame with GFP into the pEGFP-C2 vector (Clontech) to produce the construct pEGFP-$P_{40\text{-WT}}$. The variants $P_{40\text{-G10R}}$ and $P_{40\text{-I17R}}$ were then obtained by site-directed mutagenesis with the QuikChange XL kit (Stratagene).

Intracellular localization of N and P_{40}. HEK293T cells were obtained from ATCC (HEK293T/17–ATCC CRL-11268). Cell lines were routinely assayed for mycoplasma contamination. HEK293T cells were cultured in Dulbecco's modified Eagle's medium (DMEM, PAA laboratories) supplemented with 10% FCS (PerbioHyclone). For transfection, cells were grown for 24 h to a confluence of ~50% and were transfected with 0.5 µg of plasmid encoding N, GFP-$P_{40\text{-WT}}$ or both (or empty plasmid as control) with Turbofect transfection reagent (Thermo Scientific) at 4:1 ratios of reagent/DNA as recommended. After 48 h, cells were fixed in 3.7% paraformaldehyde (PFA) in phosphate-buffered saline (PBS) for 45 min and then were treated for 30 min with 50 mmol L^{-1} NH_4Cl and finally for another 40 min in 0.1% Triton X100–PBS. Immunofluorescence of N was performed with an in-house henipavirus-specific rabbit anti-N antibody (at a 1:1,000 dilution) and Alexa Fluor 555 secondary antibody (Life Technologies, cat. no. A-21430) at a 1:1,000 dilution. Validation information is available from the manufacturer's website. Anti-N antibody specificity was determined by immunofluorescence as shown and by western blot (**Supplementary Fig. 1g**). 4′,6-diamidino-2-phenylindole (DAPI) diluted in PBS containing 1% bovine serum albumin (BSA) was used for nuclear staining. After several washing steps, pictures were taken with a Zeiss 200M fluorescent microscope. Images were analyzed by Axiovision Software (Zeiss) and ImageJ software[45].

Inhibition of viral replication. All experiments with the Nipah virus were performed at INSERM Laboratoire Jean Mérieux (Lyon, France) in a BSL-4 containment laboratory. HEK293T cells were grown as described above for 24 h to a confluence of ~40%. Initially, the cells were transfected with plasmids encoding wild-type P_{40} in fusion with GFP, variants of P_{40} ($P_{40\text{-G10R}}$ or $P_{40\text{-I17R}}$) in fusion with GFP, or pEGFP alone as a control, with Turbofect reagent as described above. In each case, the amount of plasmid was varied from 2 µg to 0.125 µg. 24 h after transfection, cells were infected with NiV (Malaysian isolate UMMC1) at an MOI of 0.01. 1 h post infection (p.i.), virus inoculum was removed and replaced with DMEM medium containing 3% FCS. Culture supernatants and cell lysates were collected at 48 h p.i. for $TCID_{50}$ titration, and virus growth was assessed visually by inspection for syncytial formation. Images of GFP fluorescence were taken with a Zeiss 200M fluorescent microscope. Images were analyzed by Axiovision (Zeiss). For Kärber $TCID_{50}$ determination, serial ten-fold dilutions of viral culture supernatants were used to infect Vero E6 cells as described above and were read 48 h p.i. Significant differences were calculated with a one-way ANOVA test where applicable ($n = 6$, cell culture replicates).

24. Katoh, K. & Standley, D.M. MAFFT multiple sequence alignment software version 7: improvements in performance and usability. *Mol. Biol. Evol.* **30**, 772–780 (2013).
25. Marley, J., Lu, M. & Bracken, C. A method for efficient isotopic labeling of recombinant proteins. *J. Biomol. NMR* **20**, 71–75 (2001).
26. Wyatt, P.J. Submicrometer particle sizing by multiangle light scattering following fractionation. *J. Colloid Interface Sci.* **197**, 9–20 (1998).
27. Uversky, V.N. Use of fast protein size-exclusion liquid chromatography to study the unfolding of proteins which denature through the molten globule. *Biochemistry* **32**, 13288–13298 (1993).
28. Konarev, P., Petoukhov, M., Volchkov, V. & Svergun, D.I. ATSAS 2.1, a program package for small-angle scattering data analysis. *J. Appl. Crystallogr.* **39**, 277–286 (2006).
29. Svergun, D.I. Restoring low resolution structure of biological macromolecules from solution scattering using simulated annealing. *Biophys. J.* **76**, 2879–2886 (1999).
30. Volkov, V.V. & Svergun, D.I. Uniqueness of *ab initio* shape determination in small-angle scattering. *J. Appl. Crystallogr.* **36**, 860–864 (2003).
31. Lescop, E., Schanda, P. & Brutscher, B. A set of BEST triple-resonance experiments for time-optimized protein resonance assignment. *J. Magn. Reson.* **187**, 163–169 (2007).
32. Delaglio, F. *et al.* NMRPipe: a multidimensional spectral processing system based on UNIX pipes. *J. Biomol. NMR* **6**, 277–293 (1995).
33. Jung, Y.S. & Zweckstetter, M. Mars: robust automatic backbone assignment of proteins. *J. Biomol. NMR* **30**, 11–23 (2004).
34. Marsh, J.A., Singh, V.K., Jia, Z. & Forman-Kay, J.D. Sensitivity of secondary structure propensities to sequence differences between α- and γ-synuclein: implications for fibrillation. *Protein Sci.* **15**, 2795–2804 (2006).
35. Jensen, M.R., Salmon, L., Nodet, G. & Blackledge, M. Defining conformational ensembles of intrinsically disordered and partially folded proteins directly from chemical shifts. *J. Am. Chem. Soc.* **132**, 1270–1272 (2010).
36. Kabsch, W. Xds. *Acta Crystallogr. D Biol. Crystallogr.* **66**, 125–132 (2010).
37. Pape, T. & Schneider, T.R. HKL2MAP: a graphical user interface for phasing with SHELX programs. *J. Appl. Crystallogr.* **37**, 843–844 (2004).
38. Terwilliger, T.C. *et al.* Iterative model building, structure refinement and density modification with the PHENIX AutoBuild wizard. *Acta Crystallogr. D Biol. Crystallogr.* **64**, 61–69 (2008).
39. Adams, P.D. *et al.* PHENIX: a comprehensive Python-based system for macromolecular structure solution. *Acta Crystallogr. D Biol. Crystallogr.* **66**, 213–221 (2010).
40. Afonine, P.V. *et al.* Towards automated crystallographic structure refinement with phenix.refine. *Acta Crystallogr. D Biol. Crystallogr.* **68**, 352–367 (2012).
41. Emsley, P. & Cowtan, K. Coot: model-building tools for molecular graphics. *Acta Crystallogr. D Biol. Crystallogr.* **60**, 2126–2132 (2004).
42. Chen, V.B. *et al.* MolProbity: all-atom structure validation for macromolecular crystallography. *Acta Crystallogr. D Biol. Crystallogr.* **66**, 12–21 (2010).
43. Pettersen, E.F. *et al.* UCSF Chimera: a visualization system for exploratory research and analysis. *J. Comput. Chem.* **25**, 1605–1612 (2004).
44. Suhre, K. & Sanejouand, Y.H. ElNemo: a normal mode web server for protein movement analysis and the generation of templates for molecular replacement. *Nucleic Acids Res.* **32**, W610–W614 (2004).
45. Abramoff, M.D., Magalhaes, P.J. & Ram, S.J. Image processing with ImageJ. *Biophoton. Int.* **11**, 36–42 (2004).

© 2014 Nature America, Inc. All rights reserved.